DEM-BASED IMAGE PROCESSING METHODS FOR SAR IMAGES

Yrjö Rauste
Technical Research Centre of Finland
Itatuulentie 2 A, SF-02100 Espoo, FINLAND
Commission III

ABSTRACT

A major part of the variation in a SAR scene originates from terrain topography. It is indispensable to remove or reduce this variation to study the small differences in radar backscattering properties of various vegetation cover types. A method is described to compute the (relative) backscattering coefficients of pixels using a digital elevation model (DEM). A separation is made between the effect of the incidence angle on the size of a resolution cell and the effect of the incidence angle on the backscattering coefficient.

The method has been tested using a Seasat scene and DEM of a test site in northern Sweden. Separability of four vegetation cover classes has been tested. Differences in backscatter level between spruce-dominated, pine-dominated and deciduous forests and regenerated areas are very small. Higher areas, covered by mountain vegetation, show distinctively lower backscatter levels.

Results of the analysis show that:
- Separation of forest cover types improves with increasing incidence angles (shallow look angle);
- Two different SAR systems might be useful for forest applications: one with a relatively high frequency and shallow look angle to acquire information on vegetation layer and one with a lower frequency and steep look angle to acquire information on the underlying soil;
- An L-band SAR with steep look angle could possibly be used to derive terrain elevations for a digital elevation model.

1 INTRODUCTION

Application of microwave remote sensing techniques in forestry applications has been studied for two decades (Morain & Simonett 1967, Sieber 1985, Teillet et al 1985, Hoekman 1985 & 1987, Hirosawa et al 1987, Mougin et al 1987, and Westman & Paris 1987). Though the dominance of topographic effects has been identified as a limiting factor in the interpretation of SAR images (Drieman 1987), only few attempts have been made to overcome this limitation (Domik et al 1984, and Domik et al 1986).

The objectives of this study are to assess the utility of the images from the future SAR satellites (ERS-1, JERS-1 and Radarsat) for vegetation and forest mapping and to develop methods for computer assisted interpretation of these images. The geocoding of SAR images, which is a prerequisite for all other DEM-based

processing of SAR images, is not treated in this paper.

2 IMAGE AND MAP DATA

The SAR image data consists of a Seasat scene acquired on 20 August, 1978 at 21:35 GMT. The image, centered at (66.0 N, 17.3 E), covers an area of about 42 km by 40 km near the village of Arjeplog in Northern Sweden (figure 1). The image has a resolution of 25 m with four looks. In the SAR processing -- processing of the raw SAR signal to an image, done by FOA 3 in Linköping, Sweden -- a pixel size of approximately 16 m (in ground range) was used. The Landsat Thematic Mapper image, used as a reference, is quadrant number 2 (north-east) of scene 197-14 acquired on 25 June 1986.

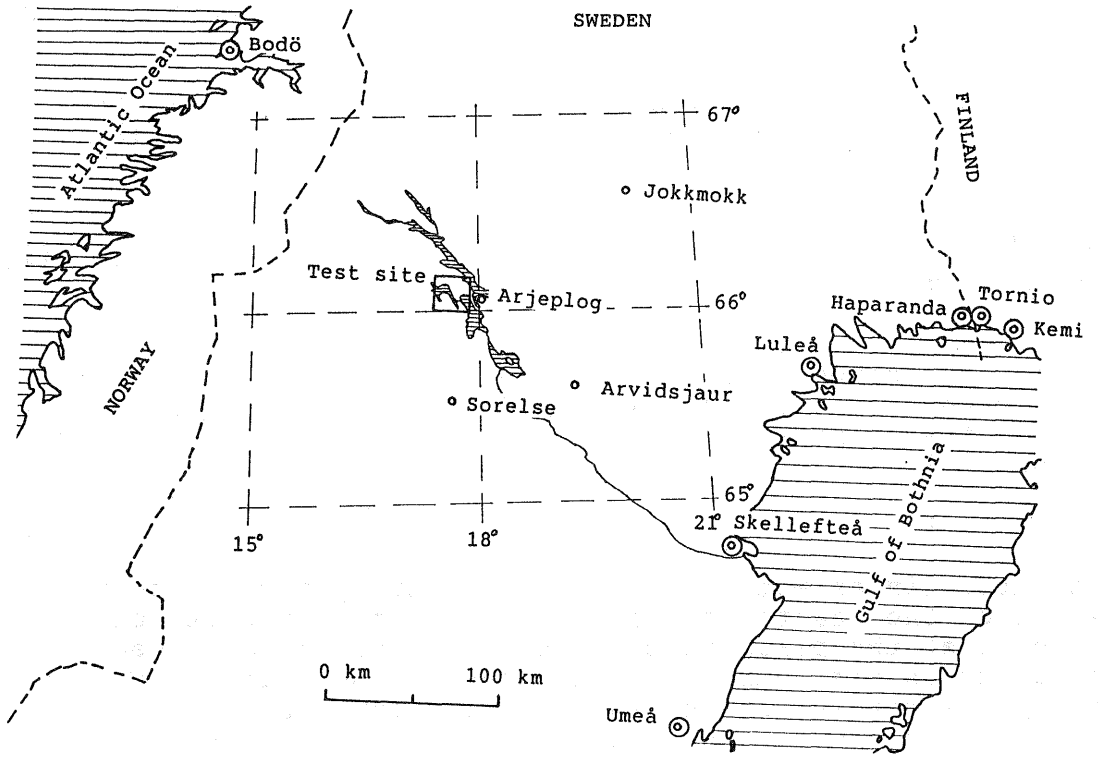

Figure 1. Location of the study area in northern Sweden.

The digital elevation model used was generated by digitizing contours of a Swedish 1:100 000 topographic map (fjäll karta). The digital elevation model covers an area of about 19 km (north) by 21 km (east) with a cell size of 25 meters. The generation of the digital elevation model was done by the Institute for Image Processing and Computer Graphics, Graz Research Center, Graz, Austria. The SAR image was geocoded using the digital elevation model (Rauste 1988).

The area covered by the digital elevation model consists of mixed forests, (mainly pine dominated), pine and spruce plantations, clear-cut areas, marshes and water bodies. There are very few

houses and agricultural fields in only one spot in the area. The stem volume of forest canopy ranges typically from zero to about 100 cubic meters per hectare (not measured). Soils are predominantly moraines with some boulders. The diameter of these boulders seldom exceeds 50 cm. Terrain elevations range from 420 m to 780 m above sea level.

3 COMPUTATION OF RELATIVE BACKSCATTERING COEFFICIENTS

The physical quantity to which a pixel value in a SAR image is related is backscattering coefficient (sometimes called differential scattering coeffiecient, Ulaby et al. 1982, p. 463). Backscattering coefficient is defined as the average value of radar cross-section per unit area. In most interpretation methods that are based on image tone the backscattering coefficient of a certain object category is considered constant and objects are classified to categories based on the differences in their backscattering coefficient.

A pixel value (or digital number) in a SAR image reperesents the power (or voltage) received from a single resolution cell. The received power is (Ulaby et al, 1982, equation 7.16):

$$\bar{P}_r = \frac{\lambda^2}{(4\pi)^3} \int \frac{P_t G^2 \sigma^0 dA}{R^4} \qquad (1)$$

Neglecting the change in slant range within a resolution cell the received power (1) can be expressed (* as a product of a system constant C, the backscattering coefficient σ°, and the area of a resolution cell A:

$$Pr = C * \sigma^\circ * A \qquad (2)$$

The resolution in azimuth direction of a SAR system is formed by intersecting the earth surface with two planes parallel to the doppler cone at the pixel in question. The distance between these planes, which is the nominal azimuth resolution, can be considered constant. The resolution in range direction is determined by intersecting the earth surface with two planes perpendicular to the propagation direction of the wavefront (i.e. perpendicular to the vector pointing to the SAR). The distance between these two planes is the slant range resolution of the SAR system, which also can be considered constant. The area of a (planar) resolution cell is:

$$A = \frac{ds}{\sin(\theta_r)} * \frac{da}{\cos(\theta_a)} \qquad (3)$$

(* This is strictly valid for uniform illumination (or response function) within a resolution cell. If we are only comparing backscattering coefficients to each other (relative backscattering coefficients) this assumption can be made for any constant point response.

where ds = the slant range resolution of the SAR,
da = the azimuth resolution of the SAR,
θ_r = the component of the incidence angle in range direction (see figure 2), and
θ_a = the component of the incidence angle in azimuth direction.

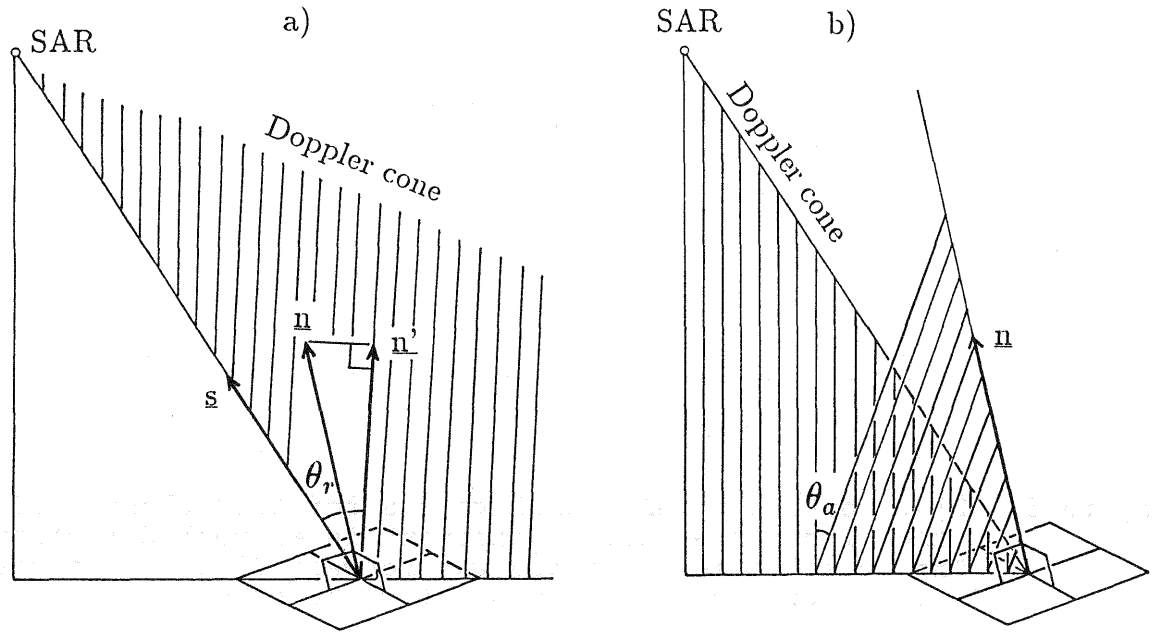

Figure 2. Definition of angles used in computation of relative backscattering coefficients. Vector $\underline{n}$ is the normal vector of a surface element, vector $\underline{n'}$ its projection onto the doppler cone and vector $\underline{s}$ is a vector pointing to the satellite. The incidence angle in range direction, θ_r is the angle between vectors $\underline{s}$ and $\underline{n'}$ (a). The incidence angle in azimuth direction θ_a (b) is the angle between the surface normal vector $\underline{n}$ and the doppler cone.

As can be seen in equation (3) the effect of θ_a on the size of a resolution cell (and on the received power) is quite different from the effect of θ_r. This can also be seen in the actual image data (figure 3).

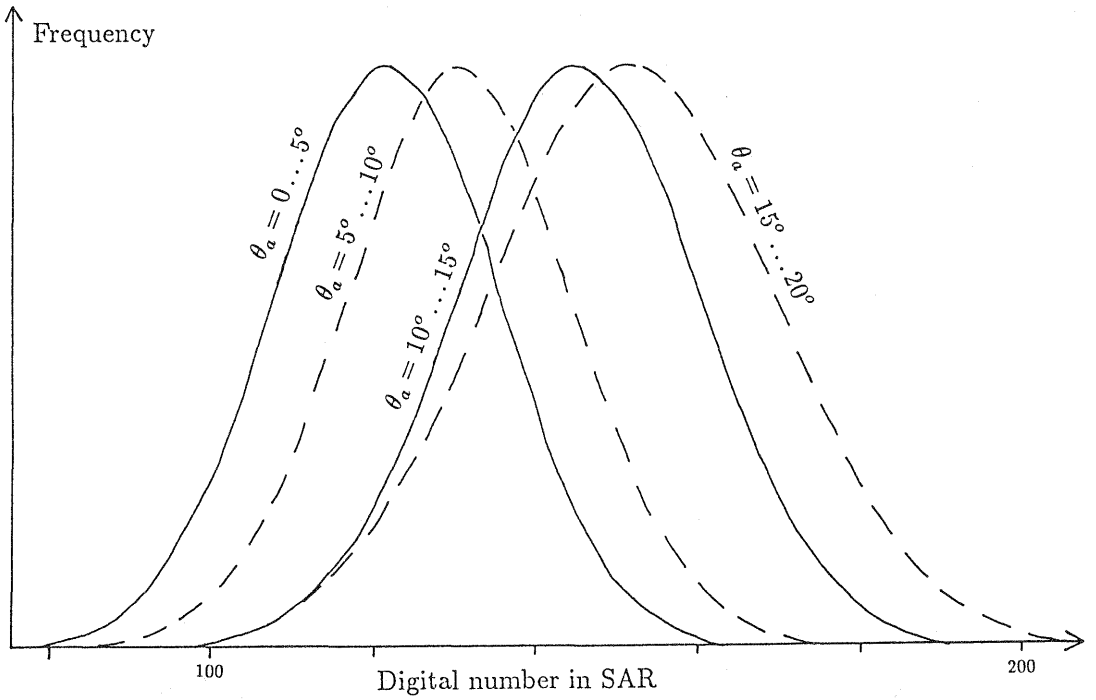

Figure 3. Distribution of SAR pixel values for four classes of θ_a (the incidence angle component in azimuth direction). The total incidence angle was between 20 and 25 degrees for all pixels used in producing the diagram.

An image showing backscattering coefficients can be computed by dividing the pixel values (or digital numbers) of the SAR image by the area (or its square root in the case of an amplitude image) of a resolution cell (3). This image is still dominated by topographic effects. A more useful image for visual interpretation is a backscatter anomaly map where modelled backscatter is subtracted from the actual backscatter. Polynomial functions can be used to model the backscattering coefficient as a function of total incidence angle. In this study a two-piece polynomial was adjusted to the observed backsactter coefficients of land pixels. A backscatter anomaly map was computed using the polynomial. The standard deviation of the output image was also forced to be uniform over the whole range of incidence angles present. The incidence angle components θ_r and θ_a were computed based on the same window and weighting function that was used in rectification of the SAR data.

3.1 Separation of Soil Component

The total backscattered power consists of two components: one originating from the ground and the other from the vegetation canopy. The separation of these components is based on the assumption that we can model one of these components and then subtract this component from the total backscatter.

There are many different modelling algorithms for the backscatter of a vegatation layer (e.g. Krul 1984). Because almost no input data for these models were available, the backscatter component of

the forest canopy was modelled only as a linear function of the stem volume per unit area. The stem volume was estimated using a Landsat Thematic Mapper image and a model developed by Tomppo (1986).

The correlation coefficient between the backscatter anomaly (in Seasat data) and the stem volume was very low (0.04) and the vegetation component very seldom exceeded 10 per cent of the total backscatter.

4 SEPARABILITY OF VEGETATION COVER CLASSES

Separability of the backscattering coefficients of four vegetation cover classes was tested using analysis of variance. The four classes are:

- spruce-dominated mixed forests,
- pine-dominated mixed forests,
- deciduous forests, and
- clear-cut or regenerated areas.

A classification map was generated (using Landsat Thematic Mapper data) to serve as ground truth data for the testing.

The separability testing was carried out separately for four incidence angle ranges and for three different SAR data sets. These data sets were generated applying different degrees of speckle reduction in geocoding. The first data set was geocoded using the nearest neighbour resampling corresponding to 4 (or slightly less) independent samples per pixel. The second data set was generated using weighted average resampling (Rauste 1988) with maximum distance 2.0 pixels. This data set corresponds to about 10 samples per pixel as derived from the ratio between the (local) standard deviation and average of the SAR image data (after reduction of the estimated system noise). The third data set was generated using weighted average resampling with maximum distance 6.0 pixels corresponding to about 160 samples per pixel.

The testing method for overall separability was analysis of variance. In pairwise tests between classes a Sokal-Rohlf test (Mäkelä 1974) was used.

The results of the class-separability tests are shown in figure 4. The risk level used in pairwise tests is 5 per cent. The test variable of the analysis of variance (F in figure 4) indicates overall separability between classes: The bigger the F-value the better overall separability between classes. The rank order (descending) of the class-means is shown above the F-value.

Separability of classes Spruce, Pine, Deciduous and Clear-cut

Incidence angle	Nearest neighbour	Lim=2.0	Lim=6.0
15° – 20°	S P D P * D * * C - * * PCSD F=10.28	S P D P * D * * C - * - PSCD F=9.49	S P D P - D - - C - - - PSCD F=2.22
20° – 25°	S P D P - D - - C * * * PSDC F=12.18	S P D P - D - - C * * * DSPC F=26.10	S P D P * D - - C * * * PDSC F=52.50
25° – 30°	S P D P * D * - C * - * SDPC F=15.96	S P D P * D * - C * * * SPDC F=48.70	S P D P * D * * C * * * SPDC F=224.60
30°–	S P D P * D * - C * * * SPDC F=25.62	S P D P * D * * C * * * SPDC F=103.04	S P D P * D * * C * * * SPDC F=238.07

Figure 4. Separability of classes Spruce (S), Pine (P), Deciduous (D), and Clear-cut (C). An asterisk (*) indicates that the average backscattering coefficients of the classes in question are separable and a hyphen (-) that the class-means are not separable.

Though the separability of class-means with 5-per-cent confidence level does not guarantee good results in a classification, the data in figure 4 show that the separability of vegetation cover types in L-band SAR data improves with increasing incidence angle and with increasing amount of speckle reduction. One vegetation cover class, mountain vegetation, was excluded from the separability tests due to lack of Thematic Mapper data. In visual analysis this class was separable from all other land classes due to its very dark tone (darker than wind-roughened water) in the backscatter anomaly map.

5 DISCUSSION

The term backscatter anomaly has been used in this study to describe essentially the same concept that Domik et al. (1984) call thematic component. This change of terminology emphasizes the fact that the topographic effects can be removed only with respect to a selected reference backscatter curve. A separate

backscatter curve can be determined for each object class but only one backscatter curve can be used when producing a backscatter anomaly map. In this study the reference backscatter curve was determined using all land pixels.

The separation between the effect of the incidence angle (components) on the size of a resolution cell and the effect of the incidence angle on the backscattering coefficient is essential in production of backscatter anomaly images (figure 3). If the existence of these two effects is neglected (and the backscatter reference curve estimated only as a function of the total incidence angle) averaging is done over the whole range of θ_a (incidence angle in azimuth direction). This is especially prominent on foreslopes. Slopes facing directly to the SAR ($\theta_a=0$) show darker tones while slopes having a larger θ_a show brighter tones. The errors are not very large. However, because the errors are very systematic and because the brighter and darker areas are systematically grouped around hills and mountains the image still seems to be influenced or even dominated by topographic effects, especially when the variation due to vegetation changes is very small (L-band SAR).

A reason for the very low backscattering coefficient of mountain vegetation could not be identified. The lack of trees does not explain this because trees are lacking also on open bogs and in clear-cut areas, which have much higher backscattering coefficients. Also the soil is rather similar to the typical moraines on lower areas. One explanation could be a thin layer of wet snow on the mountain top but this is very unlikely because the temperature on the image acquisition day was around 10 degrees Celsius.

Because the forest canopy seems to be almost transparent (the correlation between backscatter anomaly and stem volume is very low) L-band SAR with a steep look angle can reveal valuable information about the underlying ground. A SAR system with higher frequency and shallower look angle is more sensitive to the properties of vegetation canopy. For forestry applications both these aspects are important. Therefore image data from two different SAR systems could be useful.

Because the Seasat data is insensitive to vegetation, an L-band SAR with steep look angle could be used to generate the DEM data needed in processing SAR data. An algorithm could be developed that utilizes the pixel value's dependence on the components of the incidence angle, together with control information acquired using optical images or SAR data with a different look angle. Further research is needed to estimate the accuracy obtainable by this approach.

6 ACKNOWLEDGEMENTS

The study reported in this paper is part of the project SLARSAR funded mainly by the Technical Research Centre of Finland as a part of the research program of space technology. In its earlier stages the project has received support from the Academy of Finland and Neste Ltd.

7 REFERENCES

Domik, G., Kobrick, M. & Leberl, F. 1984. Analyse von Radarbildern mittels Digitaler Höhenmodelle. Bildmessung und Luftbildwesen, Volume 54 (1984), Heft 5. p. 249-263.

Domik, G., Leberl, F. & Cimino, J.B. 1986. Multiple incidence angle SIR-B experiment over Argentina: Generation of secondary image products. IEEE Transactions on Geoscience and Remote Sensing, volume GE-24, number 4, July 1986. p. 492-497.

Drieman, J.A. 1987. Evaluation of SIR-B imagery for monitoring forest depletion and regeneration in western Alberta. Canadian Journal of Remote Sensing, Vol. 13, No. 1, (July 1987), p. 19-25.

Hirosawa, H., Matsuzaka, Y., Daito, M. & Nakamura, H. 1987. Measurement of backscatter from conifers in the C and X bands. International Journal of Remote Sensing, Vol. 8 (1987), No. 11, p.1687-1694.

Hoekman, D.H. 1985. Radar backscattering of forest stands. International Journal of Remote Sensing, Vol. 6 (1987), No. 2, p. 325-343.

Hoekman, D.H. 1987. Multiband-scatterometer data analysis of forests. International Journal of Remote Sensing, Vol. 8 (1987), No. 11, p. 1695-1707.

Krul, L. 1984. Microwave remote sensing and vegetation; problems, progress and solutions, a review. Proceedings of an EARSeL workshop, Amsterdam, the Netherlands, 10-12 December 1984. ESA SP-227, p. 3-9.

Morain, S.A. & Simonett, D.S. 1967. K-band radar in vegetation mapping. Photogrammetric Engineering, Vol. XXXIII, No. 7, p. 730-740.

Mougin, E., Le Toan, T., Lopes, A., Borderies, P. & Sarremejean, A. 1987. Backscattering measurements at X-band on young coniferous trees. Proceedings of IGARSS'87 Symposium, Ann Arbor, 18-21 May 1987.

Mäkelä, Y. 1974. Tilastotiedettä biologeille. (Statistics for biologists, in Finnish). Synapsi r.y. Turku. p. 87 & 266.

Rauste, Y. 1988. Rectification of spaceborne SAR images using polynomial rectification and a digital elevation model. Photogrammetric Journal of Finland.

Sieber, A.J. 1985. Forest signatures in imaging and non-imaging microwave scatterometer data. ESA Journal, Vol. 9, p. 431-448.

Teillet, P.M., Guindon, B., Meunier, J.-F. & Goodenough, D.G. 1985. Slope-aspect effects in synthetic aperture radar imagery. Canadian Journal of Remote Sensing, Vol. 11, No. 1 (July 1985), p. 39-49.

Tomppo, Erkki. 1986. Stand delineation and estimation of stand variates by means of satellite images. Proceedings of the seminars on Remote sensing-aided forest inventory, Hyytiälä, Finland, December 10-12, 1986. Helsingin Yliopiston metsänarvioimistieteen laitoksen tiedonantoja N:o 19, (University of Helsinki, Department of forest mensuration and management, research notes No. 19). p. 59-76.

Ulaby, F.T., Moore, R.K. & Fung, A.K. 1982. Microwave remote sensing, active and passive. volume II, Addison Wesley Publishing Company, Reading Massachusetts, USA. 608 p.

Westman, W.E. & Paris, J.F. 1987. Detecting forest structure and biomass with C-band multipolarization radar: Physical model and field tests. Remote Sensing of Environment, Vol. 22 (1987), No. 2, p. 249-269.